

A coupled thermo-poroelastic analysis of wellbore stability for formations with anisotropic strengths

Weiji Liu¹ · Xiaohua Zhu¹

Received: 26 December 2015 / Accepted: 21 August 2018 / Published online: 12 September 2018
© Saudi Society for Geosciences 2018

Abstract

The temperature difference between the drilling fluid and formation will lead to an apparent temperature change around the borehole and tend to cause borehole instability problems in oil and gas drilling process. The wellbore stability models used in thinly laminated rock formations integrate the in situ stresses, pore pressure, well trajectory, and rock strength parameters to improve the wellbore stability; however, a limited amount of research has focused on the factor of formation temperature and its difference between drilling mud. Hence, a wellbore stability model is introduced based on the stress transformations and the Mohr-Coulomb failure criteria, which incorporate the rock strength anisotropy and the temperature difference between formation and drilling mud. The wellbore instability problems of anisotropic strength formation are analyzed using this model. The results show that the shear failure of rock matrix mainly occurs at two symmetric locations around the borehole and the size of failure region decreases with the inclination angle, in contrast, the shear slip failure of weak plane occurs at four locations around the borehole. The mud density required for isotropic strength should be selected as the required mud density to keep the wellbore stable if the inclination angle less than a certain value, and it almost keeps a constant with the inclination angle changes. On the contrary, the mud density required for slippage along the plane of weakness should be selected when the inclination angle larger than this value, and it is increasing with the inclination angle. Positive temperature difference will aggravate the wellbore instability, the larger the temperature difference the bigger the mud density is required.

Keywords Coupled thermo-poroelastic · Wellbore stability · Anisotropic formation · Weakness plane

Introduction

Wellbore instability problem is one of the key problems that encountered frequently during drilling process; the wellbore instability can be mainly separated into shear failure and tensile failure. In many researches, the rock mass has simply been treated as isotropic material, but in reality, the rock mass presents strongly anisotropic properties due to the existence of weakness plane or fracture plane, see Fig. 1, for these cases, using the simple isotropic stress equations to analysis of the wellbore instability problem cannot meet the needs of the drilling safety (Westergaard 1940; Reid et al. 2003; Helstrup et al. 2004; Jin et al. 2012). Hence, the analysis of wellbore

stability for formations with anisotropic strength has great engineering significance.

The anisotropic mechanical behavior of various rock types has been investigated by many researchers (Donath 1964; Chenevert and Gatlin 1965; McLamore and Gray 1967; Ramamurthy et al. 1993; Niandou et al. 1997; Ajalloeian and Lashkaripour 2000; Tien et al. 2006; Heng et al. 2015; Meng et al. 2015). Their work showed the connection of rock strength and deformation, the angle between the weakness plane and the axis of the major principal stress. Aadnoy (1988) used an anisotropic stress model to study the fracture and collapse behavior of boreholes, the model takes into account anisotropic elastic properties of rocks; the results showed that neglecting the anisotropic effects introduces an error. Ong and Roegiers (1993) discussed an anisotropic model for assessing the mechanical stability of deep borehole; the studies indicated that the stability of a wellbore is influenced significantly by rock anisotropy, rock strength, and in situ stress differentials. Wellbore stability problems

✉ Xiaohua Zhu
zxhth113@163.com

¹ School of Mechatronic Engineering, Southwest Petroleum University, Chengdu 610500, China

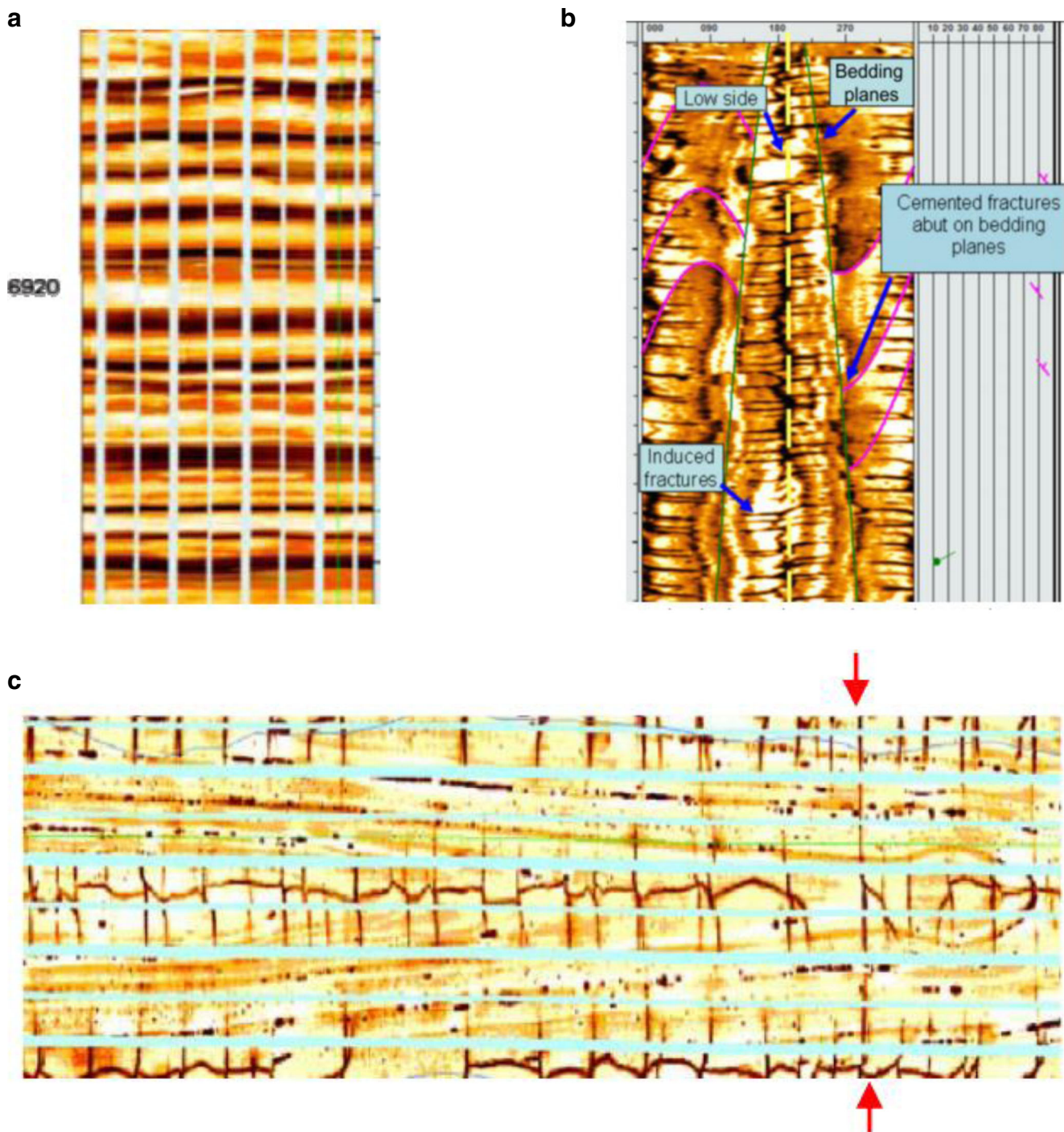


Fig. 1 Anisotropic properties of rock mass observed in drilling. **a** FMI image of an intact vertical borehole showing thin layers of the Barnett shale having contrasting resistivity (Waters et al. 2006). **b** LWD resistivity imaging log shows closely spaced induced transverse tensile fractures

intersecting two drilling induced longitudinal tensile fractures (Duncan 2009). **c** FMI image of a Barnett horizontal well drilled in the direction of the minimum horizontal stress showing fractures in both longitudinal and transverse directions (dark colors) (Waters et al. 2006)

with the pre-existing planes of weakness have been long recognized (Aadnoy and Chenevert 1987; Okland and Cook 1998; Zhang and Roegiers 2002; Willson et al. 2007; Yan et al. 2014). Lang et al. (2011) researched the wellbore stability problems when drilling along bedding planes in vertical wells. Also, the wellbore stability along

any arbitrary well trajectory in the presence of weak bedding planes was studied (Moos et al. 1998; Willson et al. 1999; Moinfar and Tajer 2013). Li et al. (2012) studied the effect of weak bedding planes, mechanical anisotropy, and time effects on the wellbore stability for horizontal wells in shale reservoirs. The borehole stability for weak

plane formation under porous flow was researched (Lu et al. 2012, 2013; Liang et al. 2014). Lee et al. (2012, 2013) developed a model in which the anisotropic rock strength characteristic is incorporated and applying this model to two case studies shows that shear failures occur either along or across the bedding planes depending on the relative orientation between the wellbore trajectories and the bedding planes. Zhang (2013) analyzed the laboratory test data of rock compressive strengths and developed a new correlation to allow for predicting uniaxial compressive strengths in weak rocks from sonic velocities. Fekete et al. (2014) and Ostadhassan et al. (2014) highlight the effect of shale bedding plane failure on wellbore stability and the angle of attack for stable drilling conditions in weak bedding planes by developing a robust tool to account for the criterion/conditions for identifying and drilling weak bedding planes. Ma and Chen (2014) developed a strength analysis method for shale rocks with multiple weak planes based on weak plane strength theories.

The wellbore stability models for thinly laminated rock formations mentioned in the above literature integrating the in situ stresses, pore pressure, well trajectory, and rock strength parameters etc., however, the factor of temperature difference is ignored. During the drilling process, there exist temperature difference between drilling mud and formation. The temperature of drilling mud is lower than the formation at the bottom of well; the wellbore rock matrix and pore medium will be shrunken due to the cooling effect of drilling mud. On the contrary, in the upper formation, the temperature of drilling mud is higher than the formation due to its heat exchange at bottom of well, the rock matrix and porous medium will be expanded, thereby disturbing the equilibrium of the stress and pore pressure around the wellbore which will cause the extraordinary wellbore instability problems. Hence, the analysis of wellbore stability which takes into account the anisotropic strength of formation and the temperature gradient has great engineering significance. In present study, a wellbore stability model is introduced based on the stress transformations and the Mohr-Coulomb failure criteria, which incorporate the rock strength anisotropy and the temperature gradient between formation and drilling mud.

Problem description

The problem to be considered in present study is the stability of a wellbore drilled into a thinly laminated anisotropic rock formation, as shown in Fig. 2. It is assumed that the plane of weakness is ubiquitously distributed in the formation, and the cross section of wellbore is analyzed. The solution of in situ stresses around wellbore can be obtained by using the thermo-poroelasticity theory, which is performed by combining the

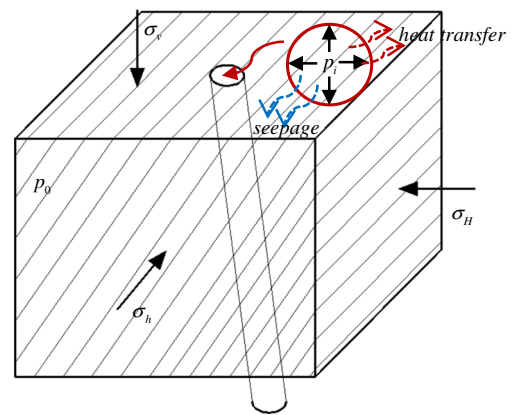


Fig. 2 A schematic drawing showing a wellbore drilled into a laminated rock formation

effect of thermal stress and differential solid/fluid expansion to rock stresses and fluid diffusion.

Thermo-poroelasticity theory

When a rock consisting of an elastic solid matrix and fluid filled pores is subjected to temperature gradient in petroleum drilling process, the solid and fluid volumes will be changed, thereby disturbing the equilibrium of the stress and pore pressure around the wellbore.

The coupled constitutive equations of poro-thermoelastic material under non-isothermal conditions of conductive heat transport have been developed by extending biot's poroelasticity theory (Biot 1941, 1955) to non-isothermal conditions (McTigue 1986, 1990; Kurashige 1989):

$$\epsilon_{ij} = \frac{1}{2G} \left[\sigma_{ij} - \frac{\nu}{1+\nu} \sigma_{kk} \delta_{ij} \right] + \frac{a(1-2\nu)}{2G(1+\nu)} \delta_{ij} p + \frac{a_m}{3} \delta_{ij} T \quad (1)$$

$$\zeta = \frac{a(1-2\nu)}{2G(1+\nu)} \sigma_{kk} + \frac{a^2(1-2\nu)^2(1+\nu_u)}{2G(1+\nu)(\nu_u-\nu)} p - \phi(a_f - a_m) T \quad (2)$$

The fluid and heat transport equations are obtained by neglecting thermal osmosis (Ghassemi et al. 2009) and heat flow by advection (Delaney 1982):

$$q_i = -\frac{k}{\mu} p_{,i} \quad (3)$$

$$h_i = -k_t T_{,i} \quad (4)$$

Following McTigue (1986, 1990), the field equations are obtained by combining the constitutive and transport equations with the force balance, mass, and heat conservation equations:

$$G u_{j,ii} + (\lambda + G) u_{i,ij} - a p_{,j} - K_m a_m T_{,j} - f_j = 0 \quad (5)$$

The fluid diffusion equation:

$$\frac{\partial p}{\partial t} - c p_{,kk} = c' \frac{\partial T}{\partial t} \quad (6)$$

The heat diffusion equation:

$$\frac{\partial T}{\partial t} - c_s T_{,kk} = 0 \tag{7}$$

The hydraulic diffusivity coefficient is as follows:

$$c = \frac{2kG(1 + v_u)^2(1-\nu)}{9(v_u-\nu)(1-\nu_u)} \tag{8}$$

The thermo-hydraulic coupling coefficient is given as follows:

$$c' = \frac{\mu c}{k} \left[\frac{2a_m(v_u-\nu)}{B(1 + v_u)(1-\nu)} + n(a_f - a_m) \right] \tag{9}$$

$$c_s = \frac{k_s}{(\rho c)_s} \tag{10}$$

$$k_s = (1-n)k_m + nk_f \tag{11}$$

$$(\rho c)_s = (1-n)\rho_m c_m + n\rho_f c_f \tag{12}$$

$$K = \frac{k\gamma_w}{\mu} \tag{13}$$

The far-field pore pressure and formation temperature are regarded as a constant, which equals to the initial pore pressure and temperature of formation, as well as the pore pressure and formation temperature at wellbore wall. The initial conditions and boundary conditions are as follows:

$$p(r, 0) = p_0, p(\infty, t) = p_0, p(r_i, t) = p_i \tag{14}$$

$$T(r, 0) = T_0, T(\infty, t) = T_0, T(r_i, t) = T_i(t) \tag{15}$$

$$p^f(r, t) = p(r, t) - p_0 \tag{16}$$

$$T^f(r, t) = T(r, t) - T_0 \tag{17}$$

According to the above equations, the stresses induced as the result of pressure and temperature changes can be calculated by the following equations (Chen et al. 2003):

$$\begin{aligned} \sigma_r' &= \frac{\alpha(1-2\nu)}{1-\nu} \frac{1}{r^2} \int_{r_i}^r p^f(r, t) r dr + \frac{Ea_m}{3(1-\nu)} \frac{1}{r^2} \int_{r_i}^r T^f(r, t) r dr \\ \sigma_\theta' &= -\frac{\alpha(1-2\nu)}{1-\nu} \left[\frac{1}{r^2} \int_{r_i}^r p^f(r, t) r dr - p^f(r, t) \right] \\ &\quad - \frac{Ea_m}{3(1-\nu)} \left[\frac{1}{r^2} \int_{r_i}^r T^f(r, t) r dr - T^f(r, t) \right] \\ \sigma_z' &= -\frac{\alpha(1-2\nu)}{1-\nu} p^f(r, t) + \frac{Ea_m}{3(1-\nu)} T^f(r, t) \end{aligned} \tag{18}$$

Stress transformations between the defined coordinate systems

We defined four reference coordinated systems: global coordinate system, GCS (N, E, Z); borehole coordinate system, BCS (x_b, y_b, z_b); cylindrical coordinate system, CCS (r, θ, z_b); weak-plane coordinate system, WCS (x_w, y_w, z_w). The relationship between the in situ stresses ($\sigma_H, \sigma_h, \sigma_v$) and GCS is defined by the maximum horizontal principal stress azimuth angle Ω ; the relationship between BCS and GCS is defined by wellbore inclination angle w and azimuth angle χ , see Fig. 3; the relationship between CCS and BCS is defined by wellbore circumferential angle θ ; the relationship between WCS and GCS is defined by dip angle of the plane of weakness ϕ and dip direction of the plane of weakness γ , just shown in Figs. 4 and 5.

The stress distribution around the wellbore for an elastic and isotropic formation in CCS is calculated by Bradley (1979):

$$\begin{aligned} \sigma_r &= \frac{r_i^2}{r^2} p_i + \frac{\sigma_{xx} + \sigma_{yy}}{2} \left(1 - \frac{r_i^2}{r^2} \right) + \frac{\sigma_{xx} - \sigma_{yy}}{2} \left(1 + \frac{3r_i^4}{r^4} - \frac{4r_i^2}{r^2} \right) \cos 2\theta + \tau_{xy} \left(1 + \frac{3r_i^4}{r^4} - \frac{4r_i^2}{r^2} \right) \sin 2\theta - \alpha p_0 \\ \sigma_\theta &= -\frac{r_i^2}{r^2} p_i + \frac{\sigma_{xx} + \sigma_{yy}}{2} \left(1 + \frac{r_i^2}{r^2} \right) - \frac{\sigma_{xx} - \sigma_{yy}}{2} \left(1 + \frac{3r_i^4}{r^4} \right) \cos 2\theta - \tau_{xy} \left(1 + \frac{3r_i^4}{r^4} \right) \sin 2\theta - \alpha p_0 \\ \sigma_z &= \sigma_{zz} - \nu \left[2(\sigma_{xx} - \sigma_{yy}) \frac{r_i^2}{r^2} \cos 2\theta + 4\tau_{xy} \frac{r_i^2}{r^2} \sin 2\theta \right] - \alpha p_0 \\ \tau_{r\theta} &= \frac{\sigma_{yy} - \sigma_{xx}}{2} \left(1 - \frac{3r_i^4}{r^4} + \frac{2r_i^2}{r^2} \right) \sin 2\theta + \tau_{xy} \left(1 - \frac{3r_i^4}{r^4} + \frac{2r_i^2}{r^2} \right) \cos 2\theta \\ \tau_{\theta z} &= \tau_{yz} \left(1 + \frac{r_i^2}{r^2} \right) \cos \theta - \tau_{xz} \left(1 + \frac{r_i^2}{r^2} \right) \sin \theta \\ \tau_{zr} &= \tau_{xz} \left(1 - \frac{r_i^2}{r^2} \right) \cos \theta + \tau_{yz} \left(1 - \frac{r_i^2}{r^2} \right) \sin \theta \end{aligned} \tag{19}$$

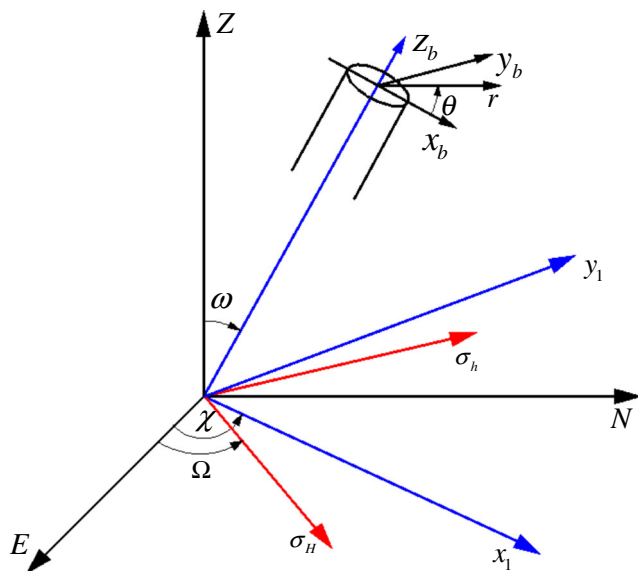


Fig. 3 Relationship between GCS and BCS (CCS, in situ stresses)

As a consequence, the total stresses induced by pore pressure, temperature gradient, and external stresses (such as in situ stresses and drilling mud pressure) can be written as the sum of Eq. 18 and Eq. 19,

$$\begin{aligned} \sigma_{rr} &= \sigma_r + \sigma_r' \\ \sigma_{\theta\theta} &= \sigma_\theta + \sigma_\theta' \\ \sigma_{zz} &= \sigma_z + \sigma_z' \end{aligned} \tag{20}$$

where:

$$\sigma_{BCS} = \begin{bmatrix} \sigma_{xx} & \sigma_{xy} & \sigma_{xz} \\ \sigma_{xy} & \sigma_{yy} & \sigma_{yz} \\ \sigma_{xz} & \sigma_{yz} & \sigma_{zz} \end{bmatrix} \tag{21}$$

The relationship between the stresses around the wellbore and in situ stresses in BCS can be expressed as follows:

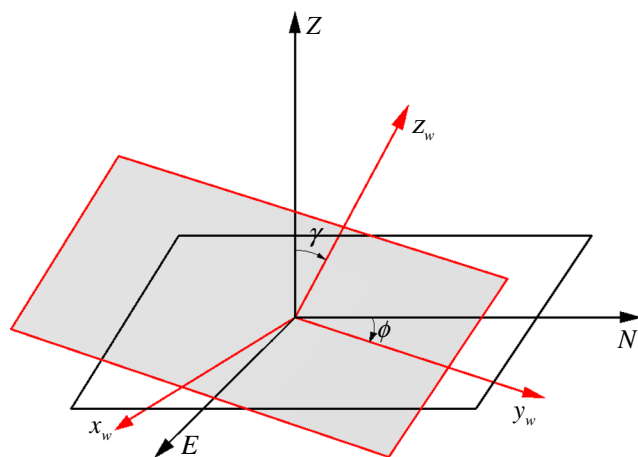


Fig. 4 Relationship between GCS and WCS

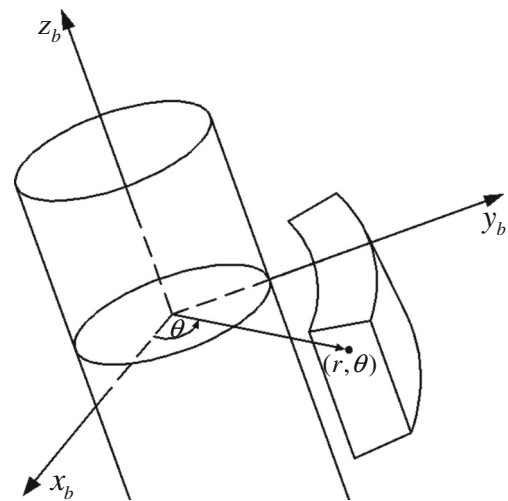


Fig. 5 Relationship between BCS and CCS

$$\sigma_{BCS} = BE^T \sigma_{in-situ} EB^T \tag{22}$$

Table 1 The impute parameters

Variables	Values
E Young's modulus	16,532 MPa
ν Poisson's ratio	0.3
λ lame constant	10,137.6 MPa
K Permeability coefficient	$1 \times 10^{-12} \text{m s}^{-1}$
n Porosity	0.1
ρ_m Solid mass density	2500 kg/m ³
α_m Solid mass thermal expansion coefficient	$1.5 \times 10^{-5}/^\circ\text{C}$
k_m Solid mass thermal conductivity	3.08 J/m s °C
c_m Solid mass specific heat	896 J/g °C
α Biot coefficient	1
k_f Pore fluid conductivity	0.58 J/m s °C
c_f Pore fluid specific heat	4200 J/g °C
α_f Pore fluid expansion	$2 \times 10^{-4}/^\circ\text{C}$
ρ_f Pore fluid density	1000 kg/m ³
γ_w Specific weight of pore fluid	$1 \times 10^4 \text{N/m}^3$
G Shear modulus	10,230.2 MPa
c_0 Cohesion of rock matrix	16.61 MPa
φ_0 Friction angle of rock matrix	32.76°
P_0 Initial pore pressure	21.48 MPa
P_i Mud pressure	25 MPa
c_w Cohesion of weak plane	5.28 MPa
φ_w Friction angle of weak plane	20.81°
ϕ Dip angle of weak plane	7°
γ Dip direction of weak plane	345°
σ_{max} Max principle stress	76.3 MPa
σ_{min} Min principle stress	55.14 MPa
σ_v overburden pressure	61.96 MPa

where E is the transformation between in situ stresses and GCS, B is the transformation between BCS and GCS, just as follows:

$$E = \begin{bmatrix} \cos\Omega & \sin\Omega & 0 \\ -\sin\Omega & \cos\Omega & 0 \\ 0 & 0 & 1 \end{bmatrix} \tag{23}$$

$$B = \begin{bmatrix} \cos\chi\cos w & \sin\chi\cos w & \sin w \\ -\sin\chi & \cos\chi & 0 \\ -\cos\chi\sin w & -\sin\chi\sin w & \cos w \end{bmatrix} \tag{24}$$

$$\sigma_{in-situ} = \begin{bmatrix} \sigma_H & 0 & 0 \\ 0 & \sigma_h & 0 \\ 0 & 0 & \sigma_v \end{bmatrix} \tag{25}$$

The stress components in CCS are expressed in Eq. (19) and Eq. (20):

$$\sigma_{CCS} = \begin{bmatrix} \sigma_{rr} & \sigma_{r\theta} & \sigma_{rz} \\ \sigma_{r\theta} & \sigma_{\theta\theta} & \sigma_{\theta z} \\ \sigma_{rz} & \sigma_{\theta z} & \sigma_{zz} \end{bmatrix} \tag{26}$$

Rock failure criteria

Failure criteria determine the amount of stress that can be tolerated by a deformation before failure. If the stresses around the wellbore are greater than the rock compression then the rock fails. There exist two shear failure forms, one is the rock matrix shear failure and the other is weakness plane shear failure.

Mohr-coulomb failure criteria for rock matrix

The Mohr-coulomb failure criterion is expressed in Eq. (27):

$$\tau_0 = c_0 + \sigma_{n0}\tan\varphi_0 \tag{27}$$

For the convenience of calculation, the eq. (27) can be written as the following form:

$$\sigma_1 = \frac{2c_0\cos\varphi_0}{1-\sin\varphi_0} + \frac{1+\sin\varphi_0}{1-\sin\varphi_0}\sigma_3 \tag{28}$$

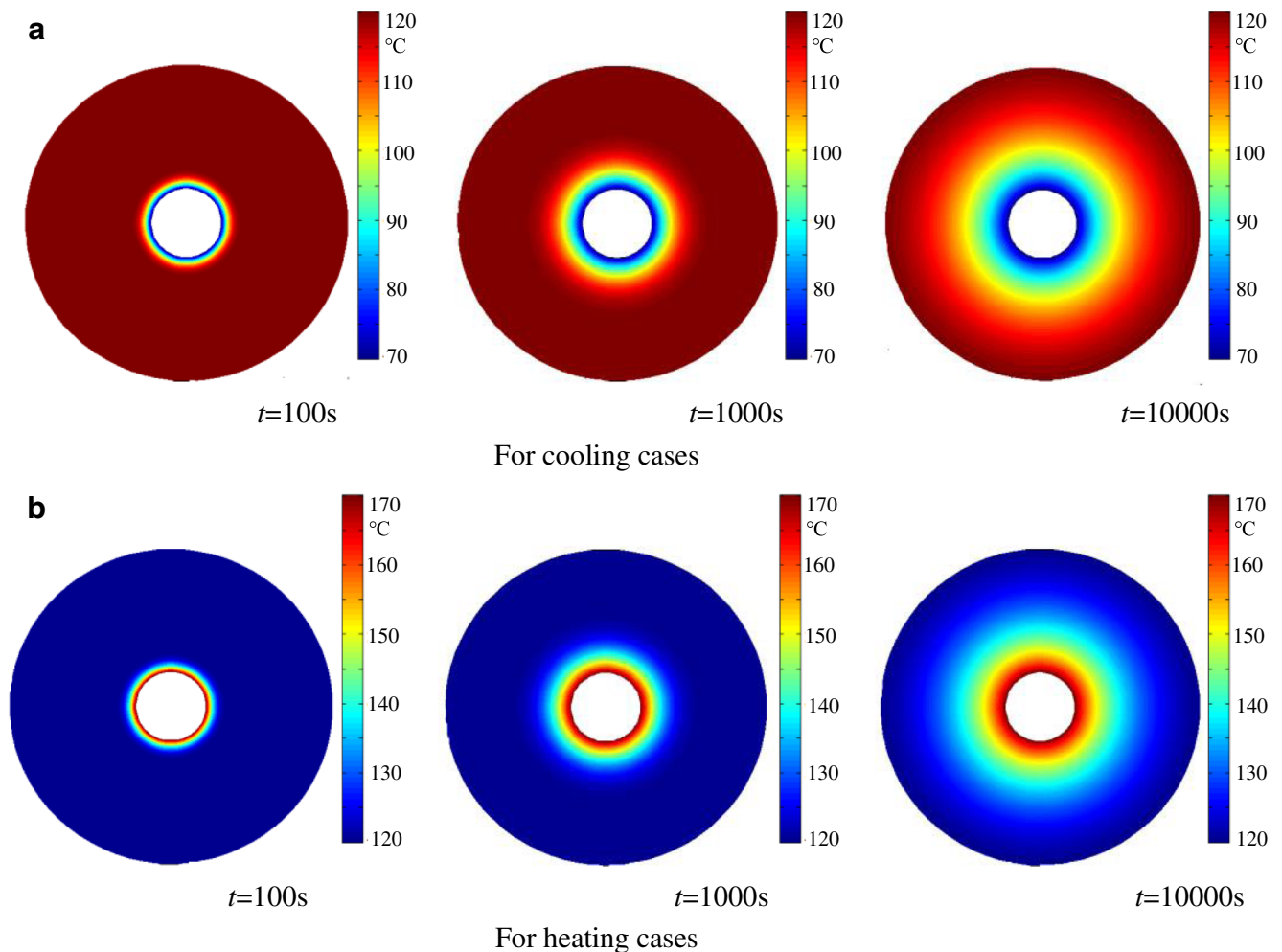


Fig. 6 Temperature profile under different caculation times

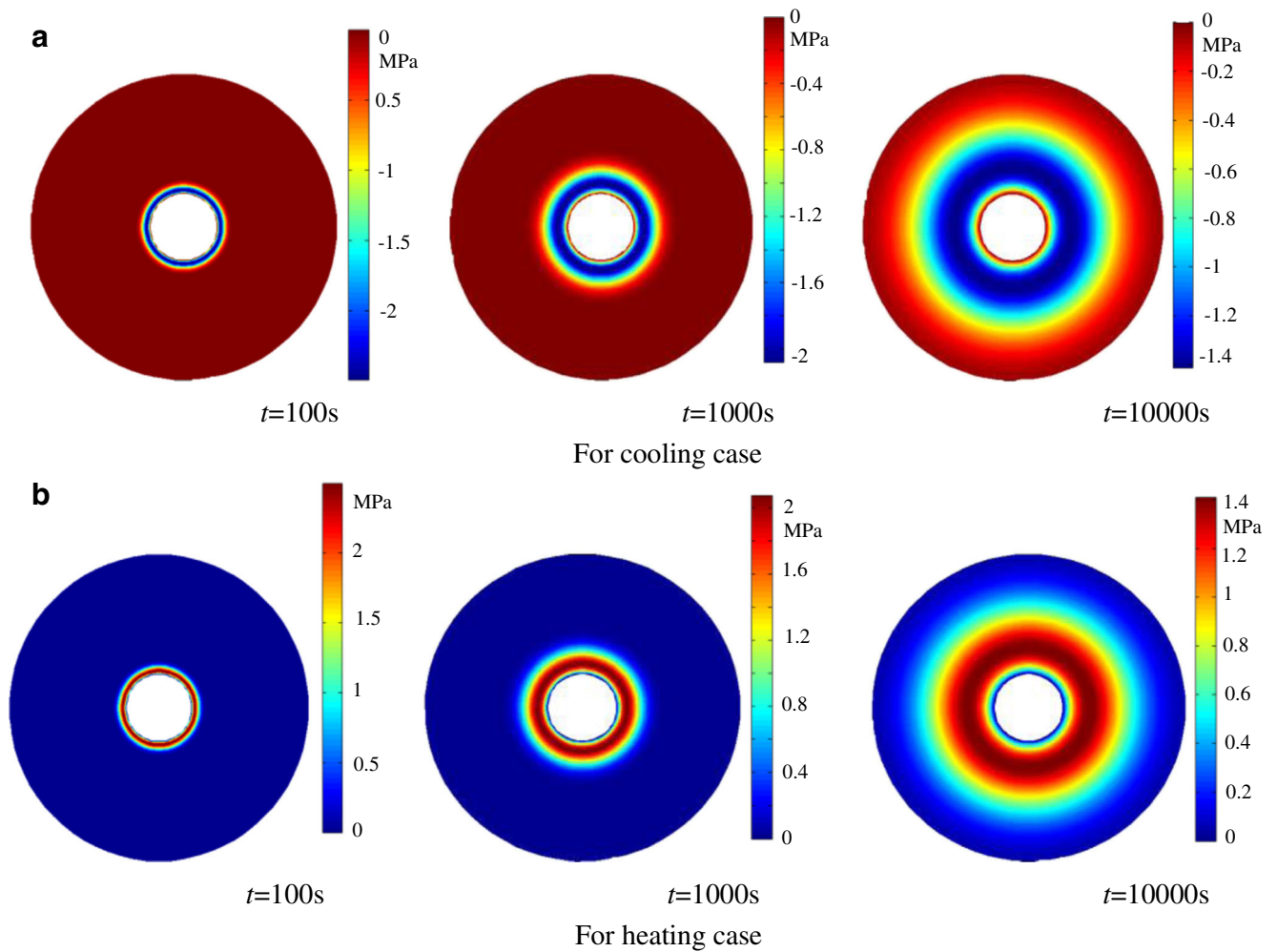


Fig. 7 Induced pore pressure distribution around the borehole under different calculation times

According to the Eq. (28), a rock matrix shear failure index is defined, it illustrates that the rock matrix of wellbore occurs shear failure if the value of c_{0f} larger than zero.

$$c_{0f} = \sigma_1 - \frac{2c_0 \cos \varphi_0}{1 - \sin \varphi_0} - \frac{1 + \sin \varphi_0}{1 - \sin \varphi_0} \sigma_3 \tag{29}$$

Fig. 8 The effect of inclination angle on rock matrix failure (azimuth angle 0°)

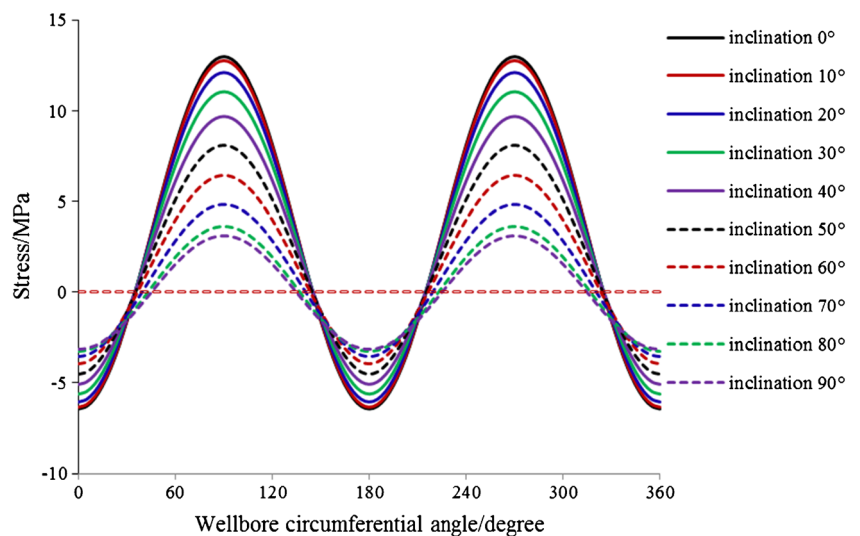
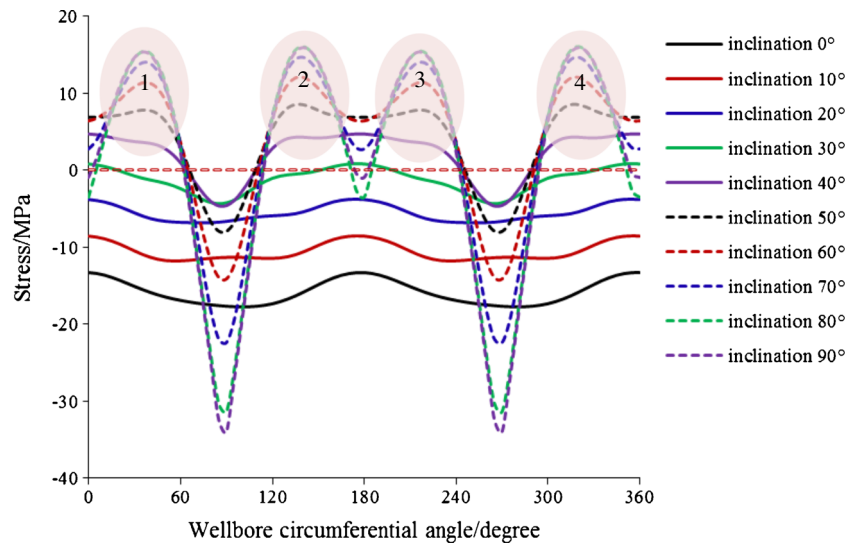


Fig. 9 The effect of inclination angle on weak plane failure (azimuth angle 0°)



The principal stresses around the wellbore wall can be calculated using the following equations:

$$\sigma_1 = \sigma_{rr}$$

$$\sigma_2 = \frac{\sigma_{\theta\theta} + \sigma_{zz}}{2} + \sqrt{\left(\frac{\sigma_{\theta\theta} - \sigma_{zz}}{2}\right)^2 + \sigma_{\theta z}^2}$$

$$\sigma_3 = \frac{\sigma_{\theta\theta} + \sigma_{zz}}{2} - \sqrt{\left(\frac{\sigma_{\theta\theta} - \sigma_{zz}}{2}\right)^2 + \sigma_{\theta z}^2}$$
(30)

$$\sigma_{Max} = Max(\sigma_1, \sigma_2, \sigma_3)$$

$$\sigma_{Min} = Min(\sigma_1, \sigma_2, \sigma_3)$$
(31)

Mohr-coulomb failure criteria for weak plane

The Mohr-coulomb failure criterion for weak plane is expressed in Eq. (32):

$$\tau_w = c_w + \sigma_{nw} \tan \varphi_w$$
(32)

We also defined a weak plane shear failure index according to the Eq. (32), the weak plane of wellbore fails if the value of c_{wf} larger than zero.

$$c_{wf} = \tau_w - c_w - \sigma_{nw} \tan \varphi_w$$
(33)

The stresses in CCS are projected onto the surface of weak plane by using Eq. (34):

$$\sigma_{CCS-WCS} = WB^T C^T \sigma_{CCS} CBW^T \sigma_{CCS-WCS} = \begin{bmatrix} \sigma_{xx}^w & \tau_{xy}^w & \tau_{xz}^w \\ \tau_{xy}^w & \sigma_{yy}^w & \tau_{yz}^w \\ \tau_{xz}^w & \tau_{yz}^w & \sigma_{zz}^w \end{bmatrix}$$
(34)

where C is the transformation between CCS and BCS and W is the transformation between WCS and GCS, just as follows:

$$C = \begin{bmatrix} \cos\theta & \sin\theta & 0 \\ -\sin\theta & \cos\theta & 0 \\ 0 & 0 & 1 \end{bmatrix}$$
(35)

Fig. 10 Wellbore failures in formations with bedding planes. **a** Wellbore buckling deformation and failure when penetrating horizontal or steeply dipping thinly-cycled beds. Model was fabricated by Bandis in 1987 (Barton 2007). **b** Laboratory tests of wellbore failure in shale with slightly dipping bedding (Okland and Cook 1998)

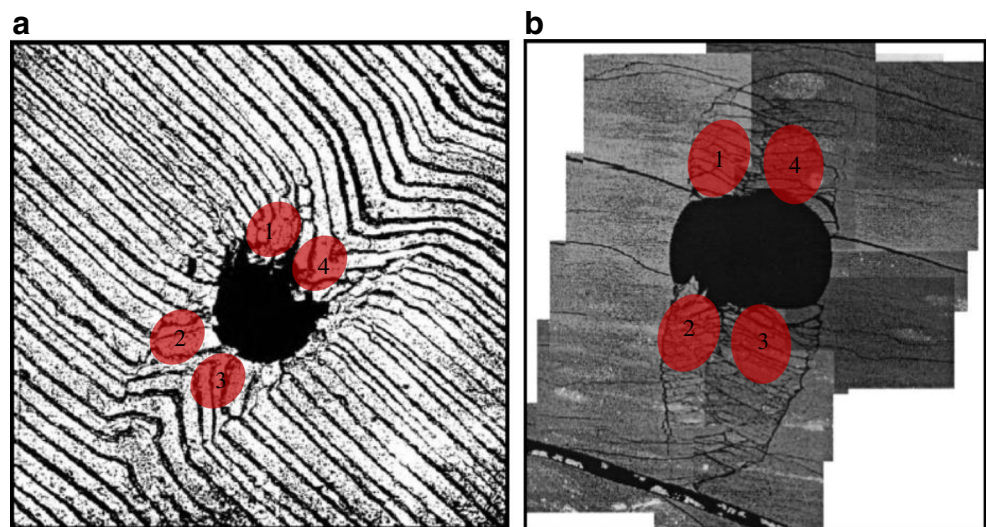
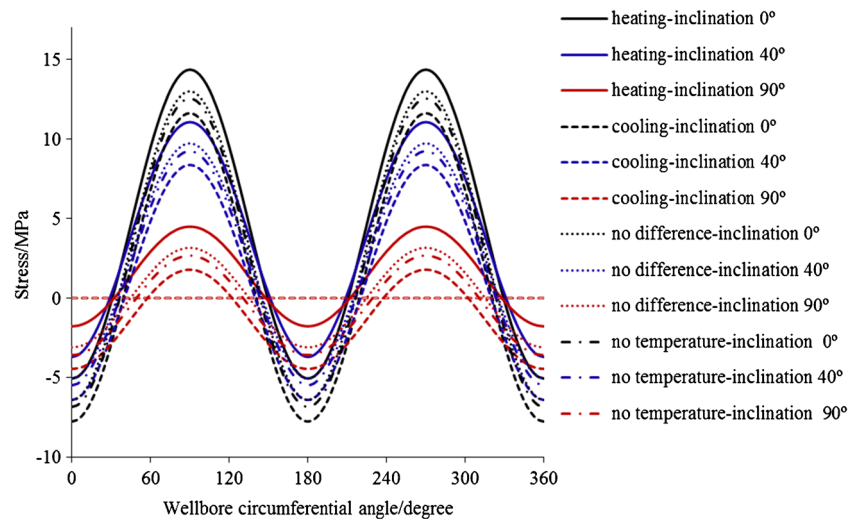


Fig. 11 The effect of temperature on rock matrix shear failure index (azimuth angle 0°)



$$W = \begin{bmatrix} \cos\gamma\cos\phi & \sin\gamma\cos\phi & \cos\phi \\ -\sin\gamma & \cos\gamma & 0 \\ -\cos\gamma\sin\phi & -\sin\gamma\sin\phi & \sin\phi \end{bmatrix} \quad (36)$$

The normal stress and shear stress on the plane of weakness are as Eq. (39).

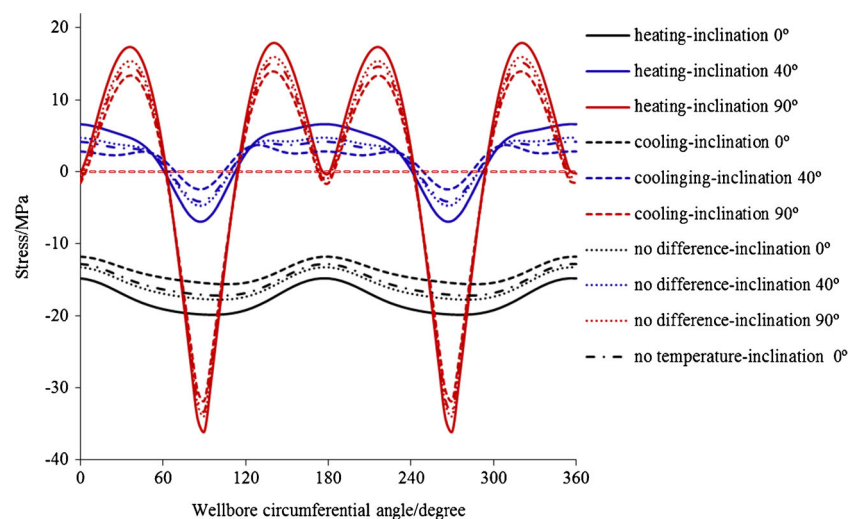
$$\sigma_{nw} = \sigma_{xx}^w \quad (37)$$

$$\tau_w = \sqrt{(\tau_{xy}^w)^2 + (\tau_{xz}^w)^2}$$

Wellbore stability analysis and discussion

The rock used in this paper is obtained from Shuanghe area in Nanbu, Sichuan Province of China; the related experimental study of the rock has been done by Chen and Ma (2014) and Jia et al. (2012); the impute parameters are shown in Table 1.

Fig. 12 The effect of temperature on weak plane shear slip failure index (azimuth angle 0°)



Transient temperature and pore pressure

The temperature profiles around the wellbore wall at different calculation times are plotted in Fig. 6. Figure 6a presents the cooling cases with a negative temperature difference, and Fig. 6b is the heating cases with a positive temperature difference. The size of the influenced area becomes larger with increasing time. For the cooling cases, the initial temperature of formation and drilling mud are 120 and 70 °C, respectively, with - 50 °C temperature difference. For the heating cases, the initial temperature of formation and drilling mud are 70 and 120 °C, respectively, with + 50 °C temperature difference.

Figure 7 presents the induced pore pressure distribution around the borehole. A significant increase of pressure is generated near the wellbore at early times for the heating cases; on the contrary, a decreased pressure is generated for the cooling cases. With the time increasing the peak of the pore pressure is reduced and moves away from the wellbore, the pore pressure of the far away wellbore is almost not been disturbed and approximately equal to the initial formation pore pressure.

Effect of inclination angle

Figure 8 presents the variation of the rock matrix shear failure index against wellbore circumferential angle for different inclination angles of wellbore. The value of shear failure index decreases with the inclination angle increases at the circumferential angle of 90° and 270° , but the contrary phenomenon occurs in 180° and 360° . The shear failure of rock matrix mainly occurs at the circumferential angle of 90° and 270° and the size of failure region decreases with the inclination angle. Figure 9 presents the variation of weak plane shear slip failure index versus wellbore circumferential angle under

various inclination angles. Just as the figure illustrated, the shear slip failure index of weak plane increases with the inclination angle increases at four locations around the borehole, the weak plane shear slip failure occurs if the value of failure index larger than zero. According to the above discussions, it can be concluded that the inclination angle has a dramatically influence on wellbore stability; in other words, wellbore stability has an intimate connection to the angle between weakness plane and the axis of borehole. In these two cases, the temperature difference between formation and drilling mud has not been taken into consideration, both of them are supposed equal to 120°C , and the calculation time is 1000 s.

Fig. 13 Failure regions various temperature difference (azimuth angle 0°)

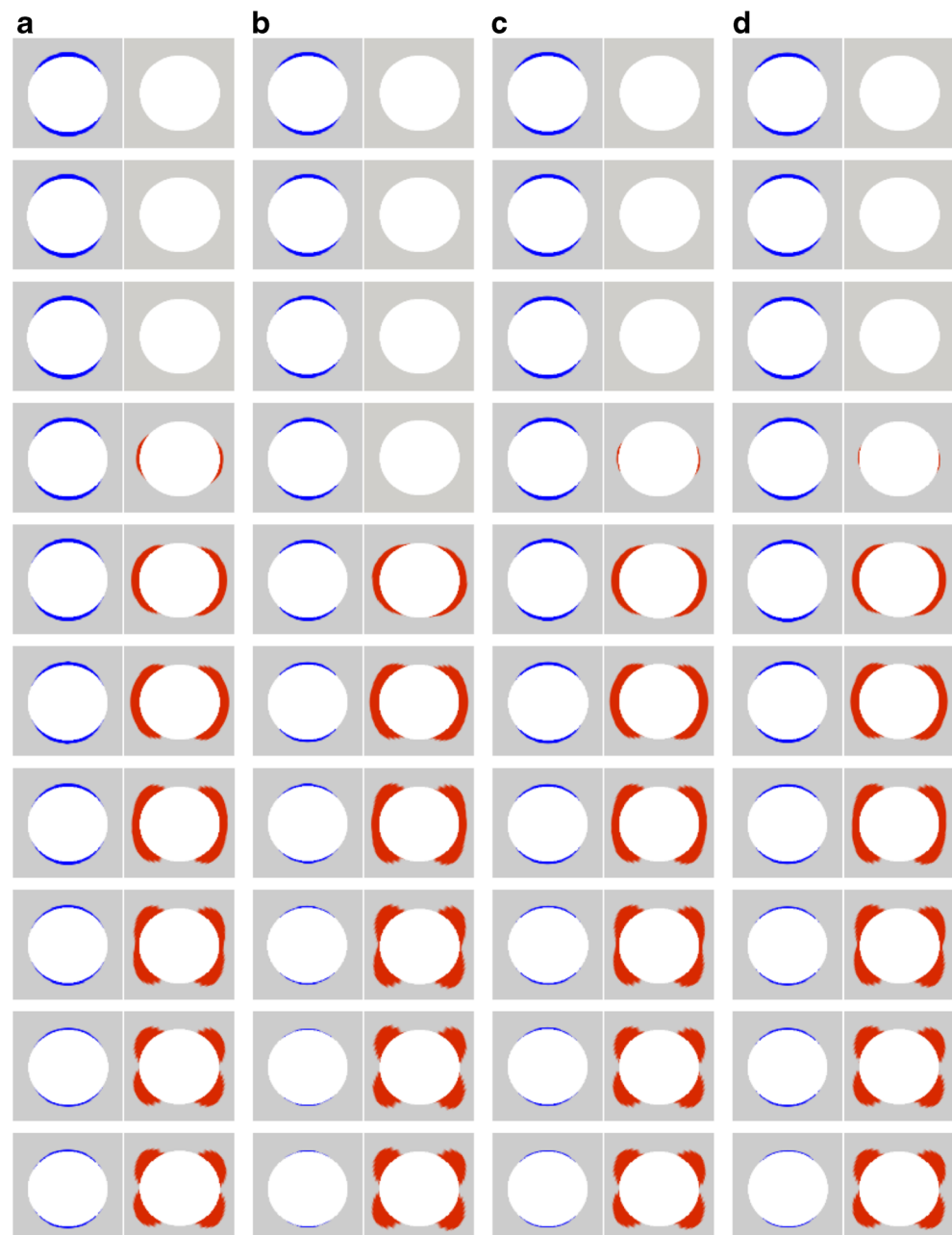


Fig. 14 Critical mud density for isotropic strength (azimuth angle 75°)

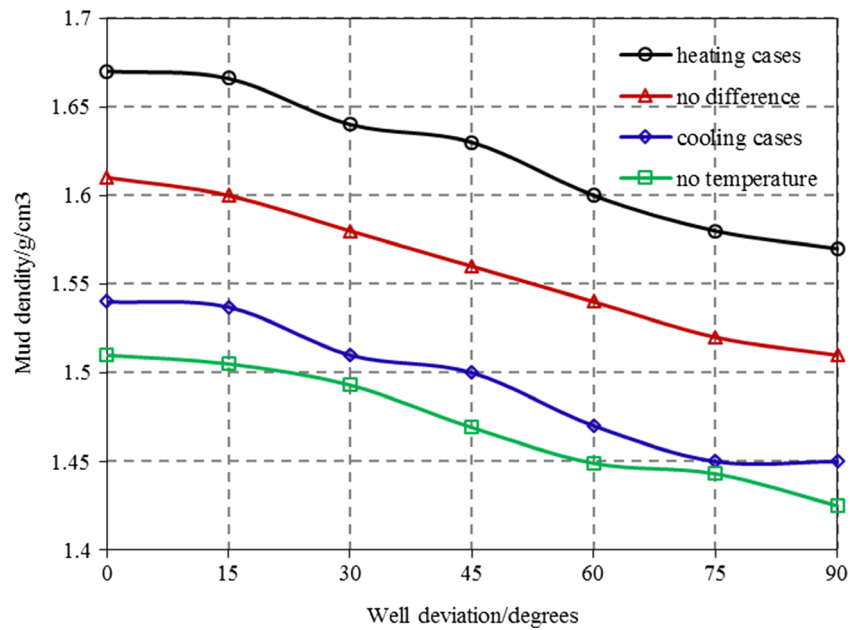
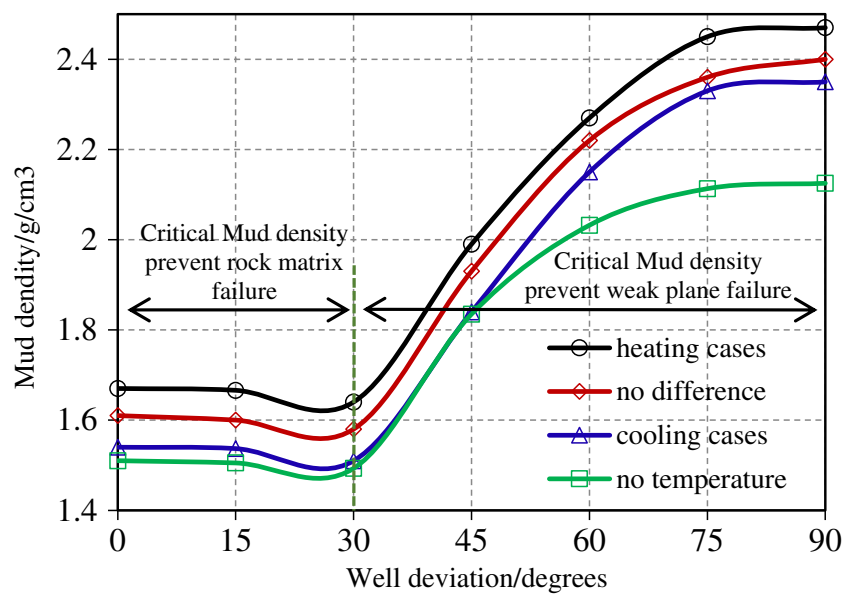


Figure 10 presents the wellbore failures in formations with bedding planes. The wellbore buckling deformation and failure when penetrating horizontal or steeply dipping thinly cycled beds which researched by Bandis (1987) and Barton (2007) are given in Fig. 10a, and the wellbore failure obtained by a laboratory tests in shale with slightly dipping bedding is shown in Fig. 10b. The wellbore failure or buckling deformation emerged at four directions around the borehole, the failure regions have been marked in the figure with the Arabic numerals. Comparing Figs. 9 and 10, the failure index proposed in this paper can accurately show the wellbore failure conditions, it also verifies the accuracy of wellbore stability model in this paper again.

Effect of temperature

Figure 11 shows the effect of temperature on rock matrix shear failure index. The formation temperature and its difference between drilling mud have an expected influence on wellbore stability, the larger the temperature difference the heavier the wellbore shear failure would be, the shear failure is more prone to occur in heating cases than it in cooling cases. The reason for this phenomenon is that the wellbore rock and pore fluid will expand due to the positive temperature gradient, increasing the compressive stress of wellbore rock and the possibility of shear failure. Figure 12 presents the effect of temperature on weak plane shear slip failure index, it shows

Fig. 15 Critical mud density for the case in which anisotropic rock strength is incorporated with the case of isotropic rock strength (azimuth angle 75°)



that the value of shear slip failure index is larger in heating cases than it in cooling cases when the weak plane is unstable; in contrast, the slip failure index is smaller in heating cases than it in the cooling cases when the weak plane is stable. The failure regions of wellbore with respect to inclination angles (range from 0° to 90° with an interval of 10°) when drilled along the azimuth angle 0° are plotted in Fig. 13. Figure 13a presents the heating cases, Fig. 13b shows the cooling cases, Fig. 13c is the cases with no temperature difference, and Fig. 13d is the cases without considering temperature. The areas shaded in blue is the rock matrix failure regions and the red represents the regions of weak plane failure. It is observed that the blue regions in heating cases are slightly larger than in cooling cases, and the weak plane presents shear slip failure when the inclination angle is 30° in heating cases;

however, the weak plane is stable in cooling. In summary, temperature has great influence on wellbore instability, the larger the temperature difference is the more unstable the wellbore will be.

The relationship between the required mud density for keeping wellbore stable and inclination angle, under four situations including heating, cooling, no temperature difference and without temperature, are presented in Figs. 14 and 15. The mud density required for both isotropic strength and slippage along the plane of weakness cases are determined for a given well azimuth and inclination, they are compared and then the larger of the two is selected as the required mud density to keep the wellbore stability. For example, for a wellbore drilled along the 75° direction with a well inclination of 45° and without considering temperature difference, the mud density

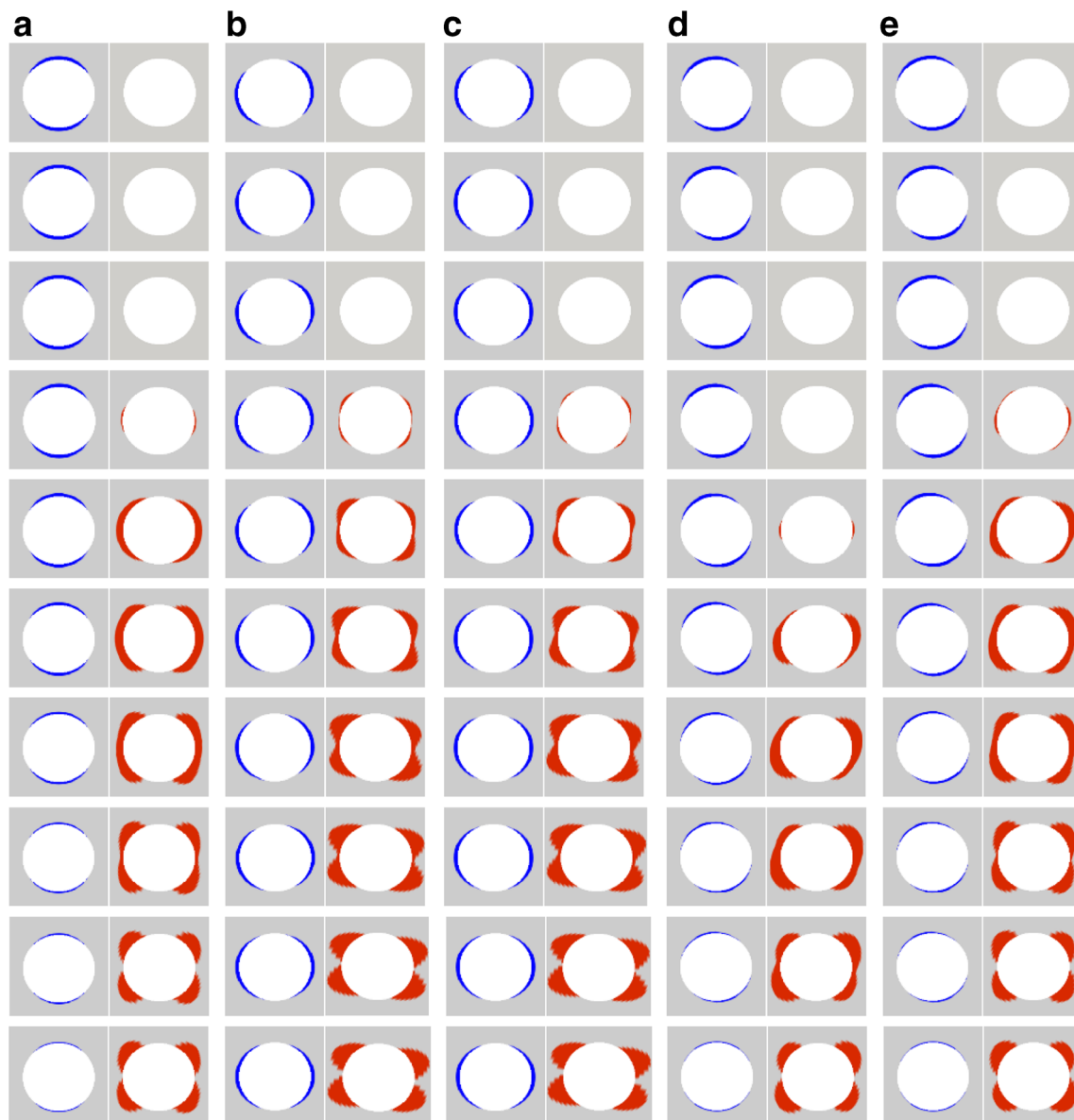


Fig. 16 Failure regions around wellbores drilled along different directions. **a** $\chi = 0^\circ$; **b** $\chi = 75^\circ$; **c** $\chi = 90^\circ$; **d** $\chi = 165^\circ$; **e** $\chi = 345^\circ$

required to prevent rock matrix failure is 1.56 g/cm^3 , whereas the mud density required to prevent weak plane shear failure is 1.93 g/cm^3 . As a consequence, the mud density required to keep wellbore stability is 1.93 g/cm^3 .

Figure 14 presents the required mud density for isotropic strength, the effect of temperature on mud density is significantly obvious. The larger the temperature difference the bigger the mud density is required to keep the wellbore stable, and the required mud density is the smallest when without considering the formation temperature; hence, the factors of formation temperature and its difference between drilling mud cannot be ignored in the analysis of wellbore instability in thinly laminated rock formations, particularly in the determination of optimal drilling mud density. The figure also illustrates the required mud density decreases with the increasing of inclination angle.

Figure 15 shows the required mud density for the case in which anisotropic rock strength is incorporated with the case of isotropic rock strength. The mud density required for isotropic strength is selected as the required mud density to keep the wellbore stable if the inclination angle small than 30° and the mud density required for slippage along the plane of weakness is selected as the required mud density to keep the wellbore stable if the inclination angle larger than 30° . The mud density of keeping wellbore stable is almost constant while the inclination angle less than 30° and then increases with the inclination.

Effect of azimuth angle

Figure 16 shows the failure regions around wellbore drilled along the direction of σ_H ($\chi = 0^\circ$), cross-dip ($\chi = 75^\circ$), σ_h

($\chi = 90^\circ$), up-dip ($\chi = 165^\circ$), down-dip ($\chi = 345^\circ$) with various wellbore inclinations under zero temperature difference condition. The wellbores drilled along the direction of σ_H ($\chi = 0^\circ$) are more stable than those in the direction of σ_h ($\chi = 90^\circ$), while the inclination angle less than a certain value the slippage along the plane of weakness will not be happened and the failure degree of rock matrix will be decreased with the increasing wellbore inclinations. It also can be seen that drilling along the up-dip direction improves wellbore stability compared to the down-dip direction and cross-dip direction, which often experienced in the field (Last et al. 1995; Skelton et al. 1995).

The variation of mud density with well inclination along different azimuth angles is shown in Figs. 17 and 18. Figure 17 presents the isotropic strength case, as described in the figure, the required mud density is the smallest while in $\chi = 0^\circ$ direction and largest in $\chi = 90^\circ$, the mud density in $\chi = 165^\circ$ direction is equal to $\chi = 345^\circ$. The required mud density decreases with the increasing of inclination angle; the change gradient of mud density in $\chi = 90^\circ$ and $\chi = 75^\circ$ directions is smaller while larger in $\chi = 0^\circ$, $\chi = 165^\circ$, and $\chi = 345^\circ$.

Figure 18 presents the case in which anisotropic rock strength is incorporated with the case of isotropic rock strength; as described in the figure, the required mud density is smaller in $\chi = 0^\circ$, $\chi = 165^\circ$, and $\chi = 345^\circ$ directions and larger in $\chi = 75^\circ$ and $\chi = 90^\circ$, the required mud density significantly increases while the well inclination is larger than 30° especially for the cases of $\chi = 75^\circ$ and $\chi = 90^\circ$. That is to say, if the formation is extensively fractured or prone to tensile failure while drilled in $\chi = 75^\circ$ and $\chi = 90^\circ$ directions, the wellbore tensile failure or leakage is more prone to take place. Therefore, drilling in $\chi = 0^\circ$, $\chi = 165^\circ$, and $\chi = 345^\circ$ directions is the best choice.

Fig. 17 The variation of mud density with well inclination along different azimuth angles for the isotropic strength case

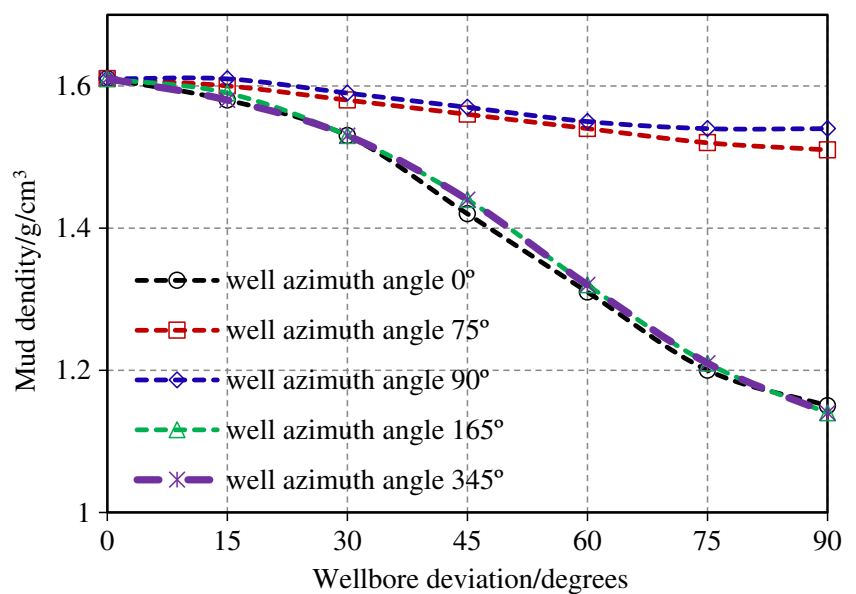
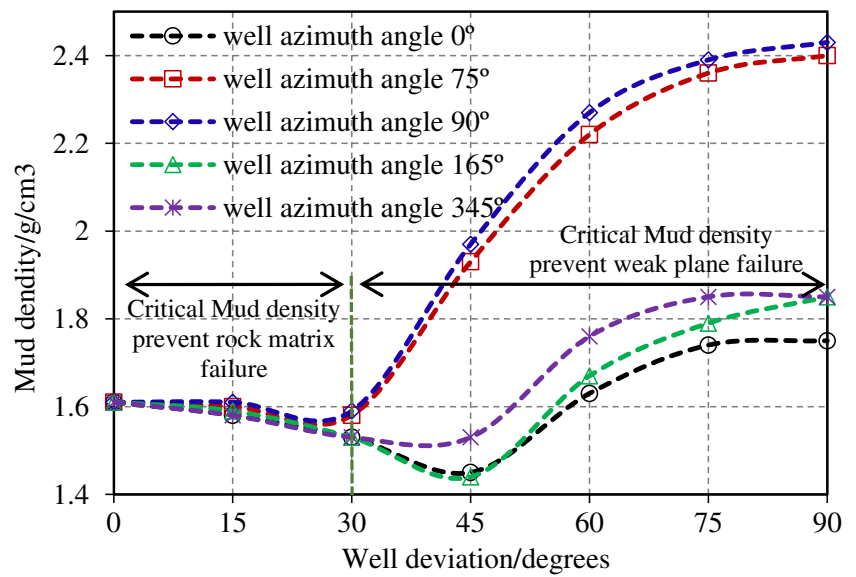


Fig. 18 The variation of mud density with well inclination along different azimuth angles for the case in which anisotropic rock strength is incorporated with the case of isotropic rock strength



Conclusions

In present study, a wellbore stability model, which incorporates the rock strength anisotropy, formation temperature, and its difference between drilling mud, is carried out based on the stress transformations between the defined coordinate systems, and the Mohr-coulomb failure criteria employed for the rock matrix and the planes of weakness. Compared to the previous models, this model is more appropriate to the reality. The wellbore instability problems of anisotropic strength formation are analyzed by using this model, the following conclusions can be drawn.

1. A significant increase or decrease of pressure will be generated near the wellbore at early times due to the temperature difference between drilling mud and formation, with the time increasing the peak of the pore pressure will decrease and move away from the wellbore.
2. The shear failure of rock matrix mainly occurs at two symmetric locations around the borehole and the size of failure region decreases with the inclination angle; in contrast, the shear slip failure of weak plane occurs at four locations around the borehole.
3. Temperature difference has a great influence on wellbore instability, positive temperature difference will aggravate the wellbore instability, the larger the temperature difference the bigger the mud density is required, and the required mud density is the smallest when without considering the formation temperature.
4. If the inclination angle less than a certain value, the mud density required for isotropic strength should be selected as the required mud density to keep the wellbore stable, and it almost keeps a constant with the inclination angle

changes. On the contrary, the mud density required for slippage along the plane of weakness should be selected when the inclination angle larger than this value, and it is increasing with the inclination angle.

5. The wellbores drilled along the direction of σ_H are more stable than those in the direction of σ_h , when the inclination angle less than a certain value the slippage along the plane of weakness will not be happened, the failure of rock matrix will be aggravated with the increasing wellbore inclination. Drilling along the up-dip direction improves wellbore stability compared to the down-dip direction and cross-dip direction.

Funding This study is supported by the National Natural Science Foundation of China (Grant No.51674214), International Cooperation Project of Sichuan Science and Technology Plan (2016HH0008), Youth Science and Technology Innovation Research Team of Sichuan Province (2017TD0014). Such supports are greatly appreciated by the authors.

Nomenclature r , Radial distance from the center of wellbore; r_i , Radius of wellbore; t , Time; T_0 , Initial formation temperature; T_i , Drilling mud temperature; P_0 , Initial formation pore pressure; P_i , Drilling mud pressure; k_m , Solid mass thermal conductivity; ν , Poisson's ratio; K , Permeability coefficient; n , Porosity; ν_u , Undrained poisson's ratio; γ_w , Specific weight of pore fluid; c , Thermo-hydraulic coupling coefficient; k_s , Rock bulk conductivity; T , Temperature; χ , Azimuth angle; σ_h , Minimum horizontal principal stress; ϕ , Dip angle of the plane of weakness; $\sigma_{xx}\sigma_{yy}\sigma_{zz}\sigma_{xy}\sigma_{yz}$, Normal and shear stresses in the borehole coordinate system; $\sigma_{wx}\sigma_{wy}\sigma_{wz}\sigma_{wx}\sigma_{wy}\sigma_{wz}$, Normal and shear stresses in the weak plane coordinate system; σ_{n0} , Normal stress; φ_0 , Friction angle of rock matrix; σ_{nw} , Effective normal stress acting on the plane of weakness; φ_w , Friction angle of the plane of weakness; $\sigma_{max}\sigma_{min}$, The max and min principal stresses; Ω , Maximum horizontal principal stress azimuth angle; k_s , Equivalent thermal conductivity; k_f , Pore fluid conductivity; α_m , Solid mass thermal expansion coefficient; α_f , Pore fluid expansion; ρ_m , Solid mass density; ρ_f , Pore fluid density; c_m , Solid mass specific heat; c_f , Pore fluid specific heat; E , Young's modulus; λ , Lamé constant; k , Permeability; G , Shear modulus; μ , Pore fluid viscosity; c , Hydraulic

diffusivity coefficient; α , Biot coefficient; p , Pore pressure; w , Wellbore inclination angle; σ_H , Maximum horizontal principal stress; σ_v , Overburden pressure; γ , Dip direction of the plane of weakness; $\sigma_{r1}, \sigma_{\theta\theta}, \sigma_{zz}, \sigma_{r\theta}, \sigma_{rz}, \sigma_{\theta z}$, Effective normal and shear stresses in the cylindrical coordinate system; τ_0 , Shear strength; c_0 , Cohesion of rock matrix; τ_w , Resultant shear stress acting on the plane of weakness; c_w , Intrinsic shear strength of the plane of weakness; $\sigma_1, \sigma_2, \sigma_3$, The principal stress in three directions; θ , Wellbore circumferential angle; c_s , Thermal diffusivity; f_b , Body force

References

- Aadnoy BS (1988) Modeling of the stability of highly inclined boreholes in anisotropic rock formations (includes associated papers 19213 and 19886)[J]. SPE Drill Eng 3(03):259–268
- Aadnoy BS, Chenevert ME (1987) Stability of highly inclined boreholes (includes associated papers 18596 and 18736) [J]. SPE Drill Eng 2(04):364–374
- Ajalloeian R, Lashkaripour GR (2000) Strength anisotropies in mudrocks[J]. Bull Eng Geol Environ 59(3):195–199
- Bandis S C, Lindman J, Barton N (1987) Three-dimensional stress state and fracturing around cavities in overstressed weak rock[C]//6th ISRM Congress. International Society for Rock Mechanics
- Barton N (2007) Rock quality, seismic velocity, attenuation and anisotropy. Taylor & Francis, Routledge
- Biot MA (1941) General theory of three-dimensional consolidation[J]. J Appl Phys 12(2):155–164
- Biot MA (1955) Theory of elasticity and consolidation for a porous anisotropic solid[J]. J Appl Phys 26(2):182–185
- Bradley WB (1979) Failure of inclined boreholes[J]. J Energy Resour Technol 101(4):232–239
- Chen P, Ma TS (2014) A collapse pressure prediction model of horizontal shale gas wells with multiple weak planes[J]. Nat Gas Ind 34(12):87–93
- Chen G, Chenevert ME, Sharma MM, Yu M (2003) A study of wellbore stability in shales including poroelastic, chemical, and thermal effects[J]. J Pet Sci Eng 38(3–4):167–176
- Chenevert ME, Gatlin C (1965) Mechanical anisotropies of laminated sedimentary rocks[J]. Soc Pet Eng J 5(01):67–77
- Delaney PT (1982) Rapid intrusion of magma into wet rock: groundwater flow due to pore pressure increases. J Geophys Res 87(B9):7739–7756
- Donath FA (1964) Strength variation and deformational behavior in anisotropic rock[J]. State of Stress in the Earth's Crust:281–297
- Duncan A. (2009) Characterization of the Barnett shale using borehole images and other tools. Presentation for AAPG 2009 mid-continent meeting-resources for the generations
- Fekete P, Dosunmu A, Anyanwu C, et al. (2014) Wellbore stability Management in Weak Bedding Planes and Angle of attack in well Planing[C]//SPE Nigeria annual international conference and exhibition. Society of Petroleum Engineers
- Ghassemi A, Tao Q, Diek A (2009) Influence of coupled chemo-poro-thermoelastic processes on pore pressure and stress distributions around a wellbore in swelling shale[J]. J Pet Sci Eng 67(1):57–64
- Helstrup OA, Chen Z, Rahman SS (2004) Time-dependent wellbore instability and ballooning in naturally fractured formations[J]. J Pet Sci Eng 43(1):113–128
- Heng S, Guo Y, Yang C, Daemen JJK, Li Z (2015) Experimental and theoretical study of the anisotropic properties of shale[J]. Int J Rock Mech Min Sci 74:58–68
- Jia S, Ran X, Wang Y et al (2012) Fully coupled thermal-hydraulic-mechanical model and finite element analysis for deformation porous media[J]. Chin J Rock Mech Eng 31(supplement 2):3547–3556
- Jin Y, Yuan J, Hou B, Chen M, Lu Y, Li S, Zou Z (2012) Analysis of the vertical borehole stability in anisotropic rock formations[J]. J Pet Explor Prod Technol 2(4):197–207
- Kurashige M (1989) A thermoelastic theory of fluid-filled porous materials[J]. Int J Solids Struct 25(9):1039–1052
- Lang J, Li S, Zhang J (2011) Wellbore stability modeling and real-time surveillance for Deepwater drilling to weak bedding planes and depleted reservoirs[C]//SPE/IADC drilling conference and exhibition. Society of Petroleum Engineers
- Last N, Plumb R, Harkness, et al. (1995) R An integrated approach to evaluating and managing wellbore instability in the Cusiana Field Colombia South America[J]. SPE annual technical conference and exhibition, 22–25 October, Dallas, Texas
- Lee H, Ong SH, Azeemuddin M et al (2012) A wellbore stability model for formations with anisotropic rock strengths[J]. J Pet Sci Eng 96: 109–119
- Lee H, Chang C, Ong SH, Song I (2013) Effect of anisotropic borehole wall failures when estimating in situ stresses: a case study in the Nankai accretionary wedge[J]. Mar Pet Geol 48:411–422
- Li Y, Fu Y, Tang G, et al. (2012) Effect of weak bedding planes on wellbore stability for shale gas wells[C]//IADC/SPE Asia Pacific drilling technology conference and exhibition. Society of Petroleum Engineers
- Liang C, Chen M, Jin Y, Lu Y (2014) Wellbore stability model for shale gas reservoir considering the coupling of multi-weakness planes and porous flow[J]. J Nat Gas Sci Eng 21:364–378
- Lu YH, Chen M, Jin Y, Zhang GQ (2012) A mechanical model of borehole stability for weak plane formation under porous flow[J]. Pet Sci Technol 30(15):1629–1638
- Lu YH, Chen M, Jin Y, Ge WF, An S, Zhou Z (2013) Influence of porous flow on wellbore stability for an inclined well with weak plane formation[J]. Pet Sci Technol 31(6):616–624
- Ma TS, Chen P (2014) Prediction method of shear instability region around the borehole for horizontal wells in bedding shale[J]. Pet Drill Tech 42(5):26–36
- McLamore R, Gray KE (1967) The mechanical behavior of anisotropic sedimentary rocks[J]. J Manuf Sci Eng 89(1):62–73
- McTigue DF (1986) Thermoelastic response of fluid-saturated porous rock[J]. J Geophys Res Sol-Ea (1978–2012) 91(B9):9533–9542
- McTigue DF (1990) Flow to a heated borehole in porous, thermoelastic rock: analysis[J]. Water Resour Res 26(8):1763–1774
- Meng L, Liang LX, Xiong J et al (2015) Experiment of fundamental physical properties and analysis of the wellbore stability on hard brittle shale [J]. Sci Technol Eng 7:34–40
- Moinfar A, Tajer E (2013) Analysis of wellbore instability caused by weak bedding-plane slippage for arbitrary oriented boreholes: theory and case study[C]//47th US rock mechanics/Geomechanics symposium. American Rock Mechanics Association.
- Moos D, Peska P, Zoback M D (1998) Predicting the stability of horizontal wells and multi-laterals: the role of in situ stress and rock properties[C]//SPE International conference on horizontal well technology, 119–130
- Niandou H, Shao JF, Henry JP, Fourmaintraux D (1997) Laboratory investigation of the mechanical behaviour of Tournemire shale[J]. Int J Rock Mech Min Sci 34(1):3–16
- Okland D, Cook J M (1998) Bedding-related borehole instability in high-angle wells[J]. SPE/ISRM Rock Mech Petroleum Eng
- Ong SH, Roegiers JC (1993) Influence of anisotropies in borehole stability[C]//international journal of rock mechanics and mining sciences & geomechanics abstracts. Pergamon 30(7):1069–1075
- Ostadhassan M O, Jabbari H, Zamiran S, et al. (2014) Wellbore instability of inclined wells in highly layered rocks Bakken case study[C]//SPE eastern regional meeting. Soc Pet Eng
- Ramamurthy T, Rao GV, Singh J (1993) Engineering behaviour of phyllites[J]. Eng Geol 33(3):209–225

- Reid P, Labenski F, Santos H (2003) Drilling fluids approaches for control of wellbore instability in fractured formations[J]. Paper SPE/IADC, 85304
- Skelton J, Hogg T W, Cross R, et al. (1995) Case History of Directional Drilling in the Cusiana Field in Colombia[J]. SPE/IADC Drilling Conference, 28 February-2 March, Amsterdam, Netherlands
- Tien YM, Kuo MC, Juang CH (2006) An experimental investigation of the failure mechanism of simulated transversely isotropic rocks[J]. *Int J Rock Mech Min Sci* 43(8):1163–1181
- Waters G A, Heinze J R, Jackson R, et al. (2006) Use of horizontal well image tools to optimize Barnett shale reservoir exploitation[C]//SPE annual technical conference and exhibition. Soc Pet Eng
- Westergaard H M (1940) Plastic state of stress around a deep well [J]
- Willson S M, Last N C, Zoback M D, et al. (1999) Drilling in South America: a wellbore stability approach for complex geologic conditions[C]// Latin American and Caribbean petroleum engineering conference. Soc Pet Eng
- Willson S M, Edwards S T, Crook A J, et al. (2007) Assuring stability in extended reach wells-analyses practices and mitigations[C]// SPE/IADC drilling conference. Soc Pet Eng
- Yan G, Karpfinger F, Prioul R, et al. (2014) Anisotropic wellbore stability model and its application for drilling through challenging shale gas wells[C]//international petroleum technology conference. International Petroleum Technology Conference
- Zhang J (2013) Borehole stability analysis accounting for anisotropies in drilling to weak bedding planes[J]. *Int J Rock Mech Min Sci* 60: 160–170
- Zhang J, Roegiers J C (2002) Borehole stability in naturally deformable fractured reservoirs-a fully coupled approach[C]//SPE annual technical conference and exhibition. Soc Pet Eng